Kovove Mater. 51 2013 241–249
DOI: 10.4149/km_2013_4_241

The effect of nozzle orifice diameter on penetration depth and mechanical properties of AISI 430/AISI 1040 dissimilar steel joined by keyhole PTA welding process

T. Teker[1]*, N. Özdemir[2]

[1] *University of Adıyaman, Faculty of Engineering, Department of Materials Engineering, 02040, Adıyaman, Turkey*
[2] *University of Fırat, Faculty of Technology, Department of Materials and Metallurgical Engineering, 23119, Elazıg, Turkey*

Received 6 May 2012, received in revised form 27 September 2012, accepted 5 November 2012

Abstract

In this study, AISI 430/AISI 1040 steel couple 10 mm thick were welded in the butt position without any pre-treatment using keyhole plasma transferred arc (KPTA) process. Welded joints were manufactured selecting constant welding speed (0.01 m min^{-1}) and two different nozzle orifice diameters (2.4 and 3.2 mm), three different welding currents (130, 135 and 140 A), at a constant plasma gas flow (1.2 l min^{-1}), a shielding gas flow (25 l min^{-1}). The microstructural changes that occurred in the interface regions of the welded samples were examined by microhardness, scanning electron microscopy (SEM), X-ray diffraction (XRD) and energy dispersive spectrometer (EDS). In order to determine mechanical properties of samples, the V-notch Charpy tests were performed. In addition, fracture types in the notch impact strength tests of samples were determined from the fractographic examinations using SEM.

K e y w o r d s: plasma transferred arc welding, keyhole, AISI 430, AISI 1040, nozzle orifice diameter

1. Introduction

Plasma transfer arc welding (PTAW) can be defined as a gas-shielded arc welding process where the melting of metals is achieved via the heat transferred by an arc that is created between a tungsten electrode and a workpiece. The arc is constricted by a copper alloy nozzle orifice to form a highly constricted arc column. The PTAW process can be used in two distinct operating modes, often described as the melt-in-mode and the keyhole mode. The keyhole mode of plasma is the primary attribute of that makes them penetrate thicker pieces with a single pass [1]. Compared to laser beam welding and electron beam welding, keyhole mode of plasma transfer arc welding (KPTAW) is more cost effective and more tolerant of joint preparation, though its energy is less dense and its keyhole is wider. On the other hand, KPTAW offers significant advantages over conventional gas tungsten arc welding (GTAW) in terms of penetration depth, joint preparation and thermal distortion [2, 3]. Thus, KPTAW has found applications on the welding of structural steels, automobiles, airplanes, rockets, space shuttles, and possibly on welding in space [4–8]. In KPTAW, the quality of the weld depends on the keyhole stability, which itself depends on a large number of factors, especially the physical characteristics of the material to be welded and the welding process parameters to be used [9, 10]. Thus, KPAW is susceptible to the variation of welding process parameters, which makes it have narrower range of applicable process parameters for good weld quality. The temperature profile around the keyhole and weld pool has great influence on the formation and stability of keyhole [11]. With a proper combination of orifice gas flow, travel speed and welding current, keyhole forming is possible, allowing higher welding speeds than GTAW with full penetrations. In literature, limited research has been made on the welding of AISI 430 and AISI 1040 steel. Urena et al. [12] investigated weld-

*Corresponding author: tel.: +90 416 2233800; fax: +90 416 2233812; e-mail address: tteker@adiyaman.edu.tr

Table 1. Chemical composition of test materials

Material	Chemical composition (wt.%)									
	Fe	C	Cr	Ni	Si	Mo	S	Mn	Cu	P
AISI 430	82.644	0.048	16.02	0.022	0.44	0.016	0.002	0.610	–	–
AISI 1040	97.9	0.391	–	–	0.158	–	0.022	0.655	0.310	0.034

Table 2. The process parameters used in KPTA welding

Sample No.	Welding current (A)	Plasma gas flow ($l\,min^{-1}$)	Shielding gas flow ($l\,min^{-1}$)	Welding speed ($m\,min^{-1}$)	Nozzle diameter (mm)
S1	130	1.2	25	0.01	2.4
S2	135	1.2	25	0.01	2.4
S3	140	1.2	25	0.01	2.4
S4	130	1.2	25	0.01	3.2
S5	135	1.2	25	0.01	3.2
S6	140	1.2	25	0.01	3.2

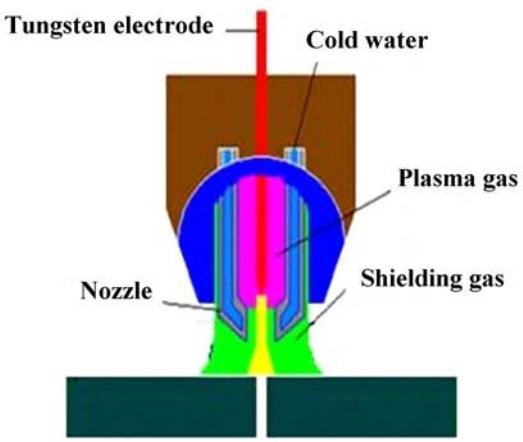

Fig. 1. Schematic presentation of the keyhole plasma transfer arc welding system.

ability of a 2205 duplex stainless steel using plasma arc welding. It was produced by keyhole PAW to have higher penetration/width ratios than welds produced in the melt-in mode.

In the present study, AISI 430 and AISI 1040 dissimilar steels of 10 mm thickness were welded in butt position without any pre-treatment using the KPTA welding process with different nozzle orifice diameters. The aim of this study was to investigate the effect of nozzle orifice diameter on the keyhole size, penetration depth, and mechanical behaviour.

2. Materials and methods

AISI 430 ferritic stainless steel and AISI 1040 dissimilar steel of $100 \times 50 \times 10\,mm^3$ were welded in the butt position without any pre-treatment using the KPTA welding process. The chemical composition of test materials is listed in Table 1. Pure argon gas was used as both the shielding gas and the plasma gas. The flow rate of the shielding gas was $25\,l\,min^{-1}$, the flow rate of the plasma gas was $1.2\,l\,min^{-1}$, diameter of the nozzle orifice was 2.4 and 3.2 mm. A schematic representation of the KPTA welding system is shown in Fig. 1, and the process parameters for keyhole welding are given in Table 2. For metallographic examination, samples were cut transversely through the joint using a low-speed saw. The cross-sections of these joints were metallographically polished using diamond paste of 3 μm as a final polish and then cleaned using acetone. For microstructural examination, AISI 1040 sides of the welded samples were etched in a solution of 2 % HNO_3 + 98 % alcohol, and specifically, AISI 430 sides were etched electrolytically in a solution of 50 % HCl + 30 % H_2O + 20 % HNO_3. The microstructural properties in the welded interface of the samples were examined by scanning electron microscopy (SEM: JEOL JSM 7001F) device. Energy dispersive spectrometry (EDS) analysis was done by JEOL JSM 7001F SEM type device to pick up the elementary contents of phases which were formed at the interface of the welded samples. In order to determine the phases and compounds on samples, XRD analysis was carried out through SHIMADZU XRD-6000 equipped with a Cu Kα/tube, wavelength of (α =) 1.54056 Å, voltage of 40 kV and current of 40 mA. The microhardness and notch impact tests were carried out. Microhardness measurements were performed by a Leica MHT-10 microhardness testing machine using a typical Vickers tip under a load of 50 g for 15 s. Impact test samples were prepared with dimensions of $55 \times 10 \times 10\,mm^3$, then the samples were tested using a Wolpert PW30

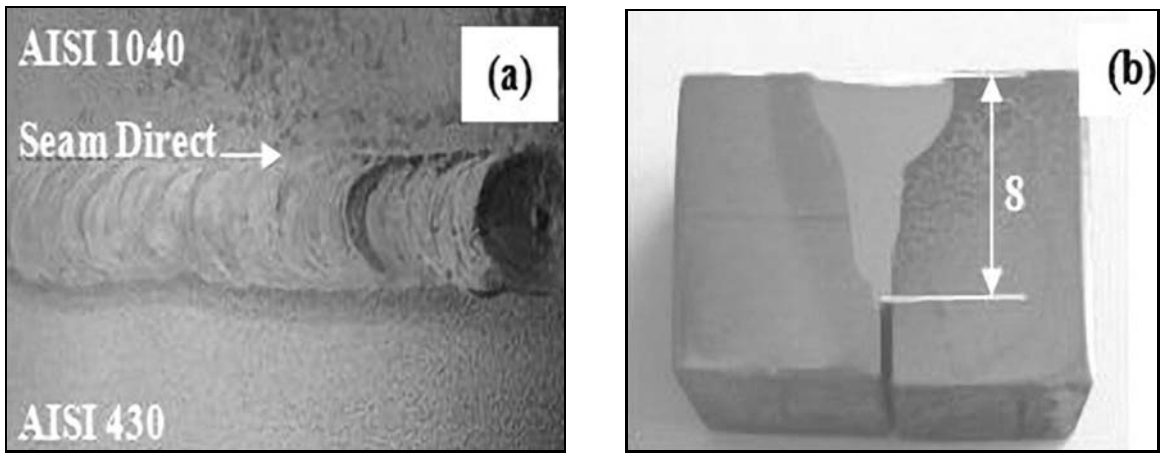

Fig. 2. a) The surface appearance of the sample S3, and b) the cross-sectional macro appearance of the sample S3.

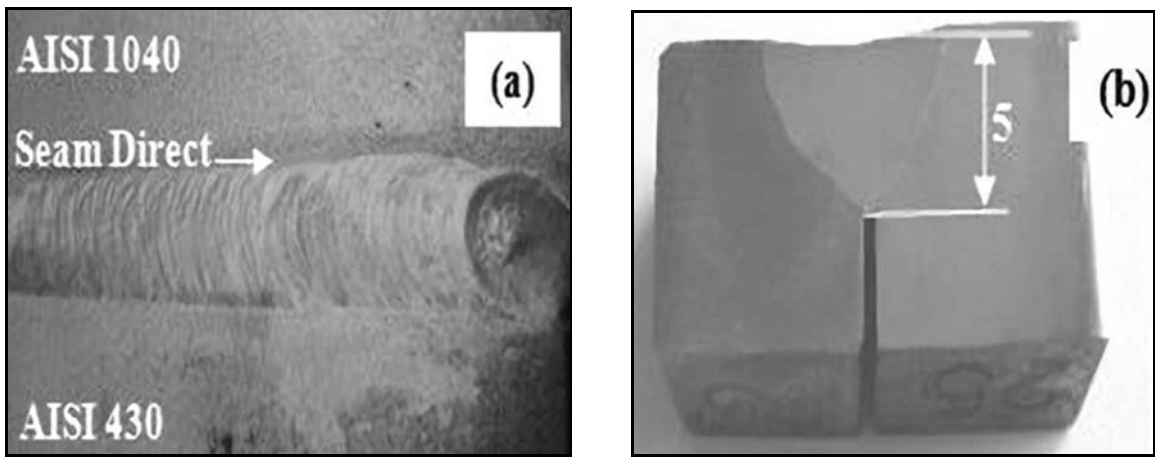

Fig. 3. a) The surface appearance of the sample S6, and b) the cross-sectional macro appearance of the sample S6.

V-notch impact strength test device with a hammer of 300 J.

3. Results and discussion

3.1. Microstructure characterization

Figures 2a,b show penetration depth and width of weld metal cross section of samples welded by keyhole PTA process using three different welding currents, and constant nozzle orifice diameter of 2.4 mm. As can be seen in the figures, the width of weld metal surface in the samples S1, S2 and S3 is approximately 7.70, 8.70 and 10.5 mm for the nozzle orifice diameter of 2.4 mm, respectively. The penetration depths of samples S1, S2 and S3 were obtained as 7, 7.5 and 8 mm, respectively (Fig. 2). By the increase of the welding current, obtained higher heat input leads to a greater increase in the volume of weld metal [11, 13]. Figures 3a,b show penetration depth and width of the weld metal surface of samples joined by keyhole PTA process using three different welding currents, and a constant nozzle orifice diameter of 3.2 mm. As can be seen in the figures, the values of width of weld metal surface in the samples S4, S5 and S6 are approximately 10.20, 11 and 11.5 mm for the nozzle orifice diameter of 3.2 mm, respectively. The values of penetration depth of samples S4, S5 and S6 were obtained as 3, 4 and 5 mm, respectively (Fig. 3). These results show that the nozzle orifice diameter and energy input are noteworthy parameters in the KPTAW. In the nozzle orifice diameter of 2.4 mm, the plasma column is more narrow and intensive than in that of 3.2 mm. Therefore, the welding penetration is higher. According to our results, the penetration depth of the samples decreased with the increase of nozzle orifice diameter. The highest penetration depth was obtained for the welded joints S1, S2 and S3 with nozzle orifice diameter of 2.4 mm. The weld metal that existed in the interface was produced using higher heat inputs, and smaller nozzle orifice diameter formed a keyhole profile.

Figure 4 shows an optical image of microstructural

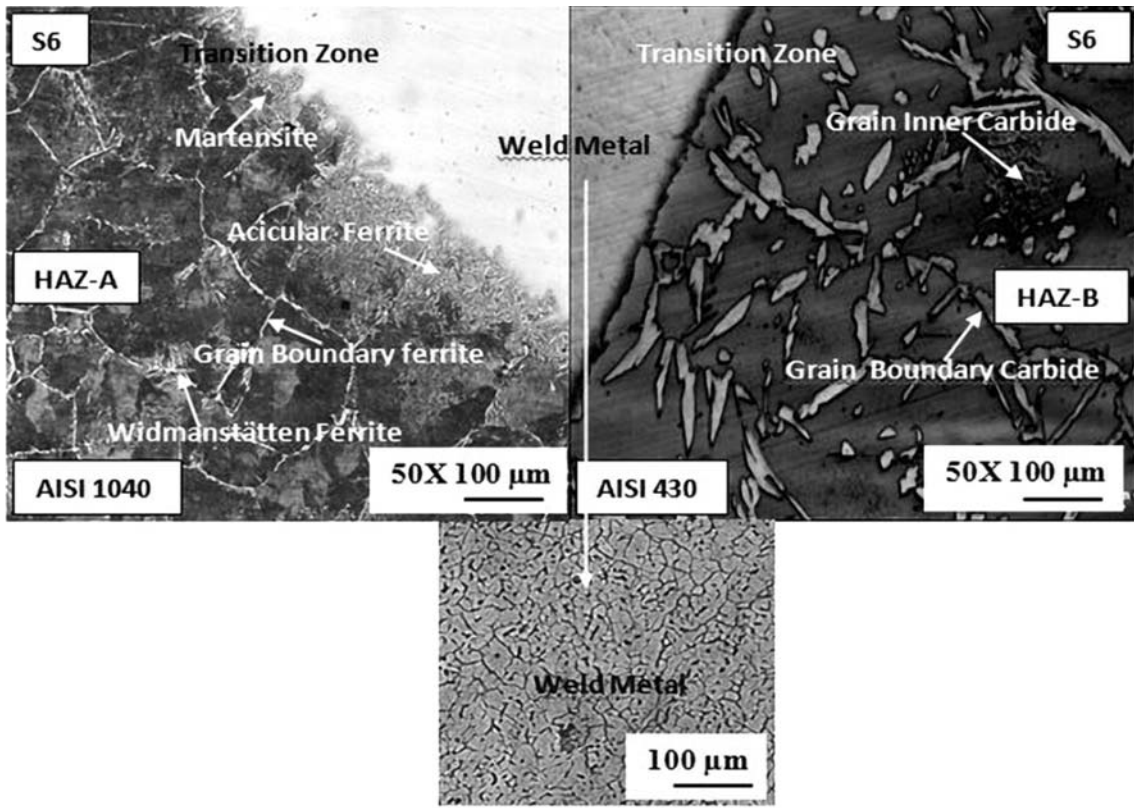

Fig. 4. Optical micrographs taken from the welding interface of the sample S6.

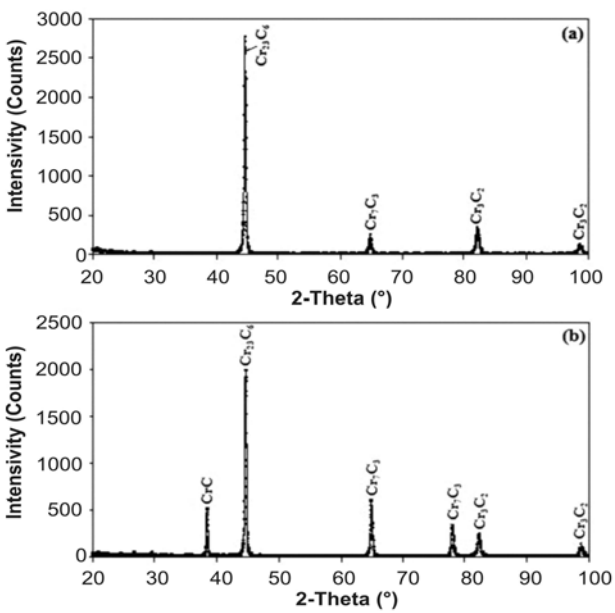

Fig. 5. XRD analysis results of KPTA welded samples: a) S3, b) S6 samples.

changes occurred at the interface of these welded joints (adjacent to the weld zone HAZ-A = AISI 1040 side and HAZ-B = AISI 430 side, weld metal). Examining the microstructure images taken from the weld interface of the welded joints, the occurred structures were observed to be quite similar, and cracks, cavities and non-welded interfaces were not observed in both transition zones adjacent to the weld zone. On the HAZ-A side, where heat input led to grain coarsening due to its annealing effect, existed plenty of acicular ferrite islands and numerous widmanstatten ferrite, lath and plate-type martensite. Acicular ferrites were generally formed on the fusion boundary and free surfaces of the material, where the cooling rate was higher. On the HAZ-B side, the zone containing coarse grains which comprised of ferrite phases and chromium carbides, also included intense amount of chromium carbide in specifically intergranular (pepper-like) and grain boundary (lath type) forms, as shown in Fig. 4.

Results of XRD analysis for the welded joints S3 and S6 are shown in Figs. 5a,b, respectively. From the results of XRD analysis, CrC, $Cr_{23}C_6$, Cr_7C_3 and Cr_3C_2 compounds were seen on the fusion zone (weld metal) of welded joints. The phase and compounds intensity occurred in the sample S6 is increased depending on the higher energy input in the nozzle orifice diameter of 3.2 mm. SEM micrographs and EDS analysis of the welded joint S3 and S6 are presented in Figs. 6 and 7. Point 1 (on AISI 1040 side), point 2 (fusion zone), point 3 (weld metal), point 4 (fusion zone) and point 5 (on AISI 430 side) are marked as the EDS analysis points. EDS analysis results of samples

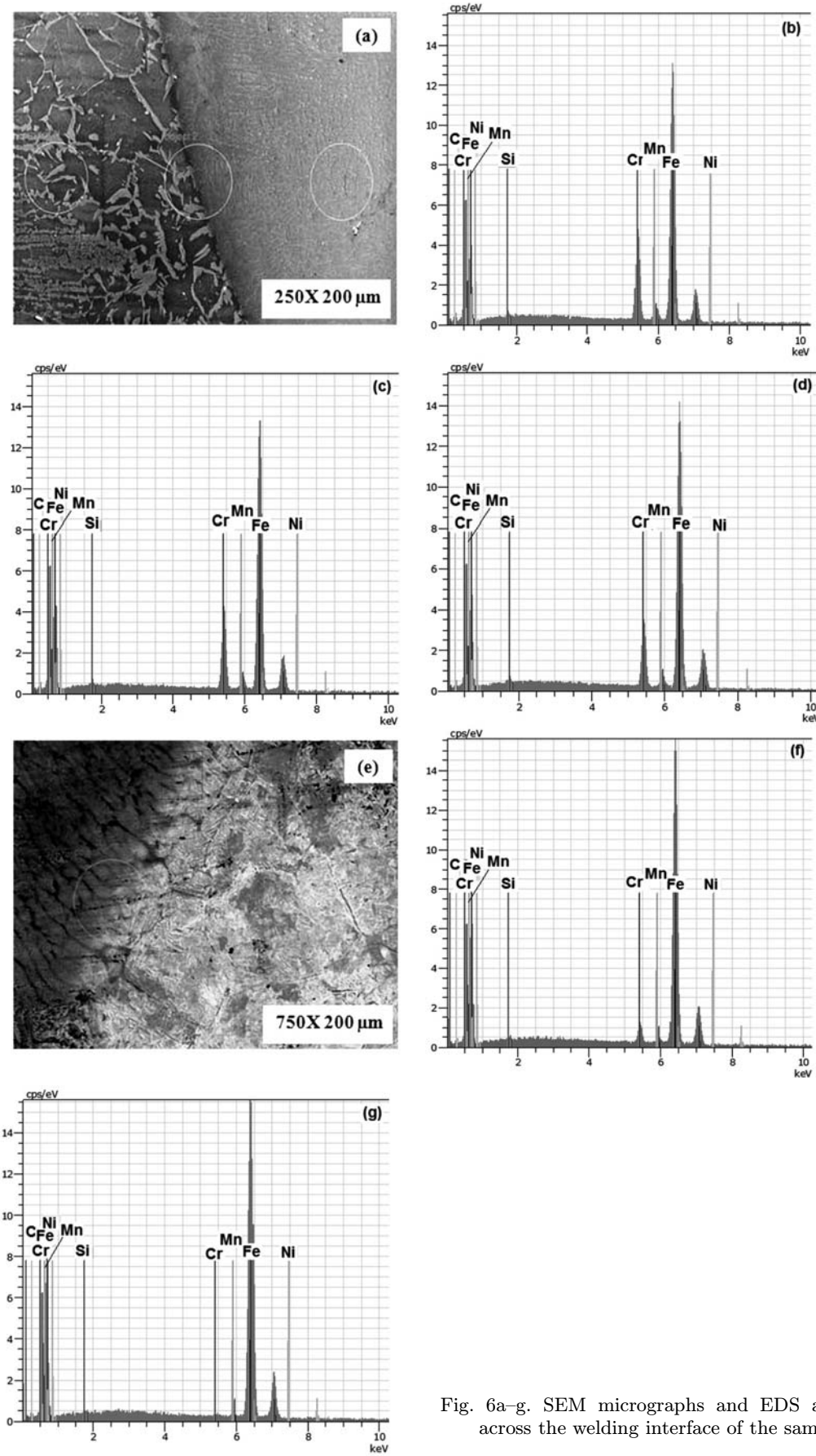

Fig. 6a–g. SEM micrographs and EDS analysis points across the welding interface of the sample S3.

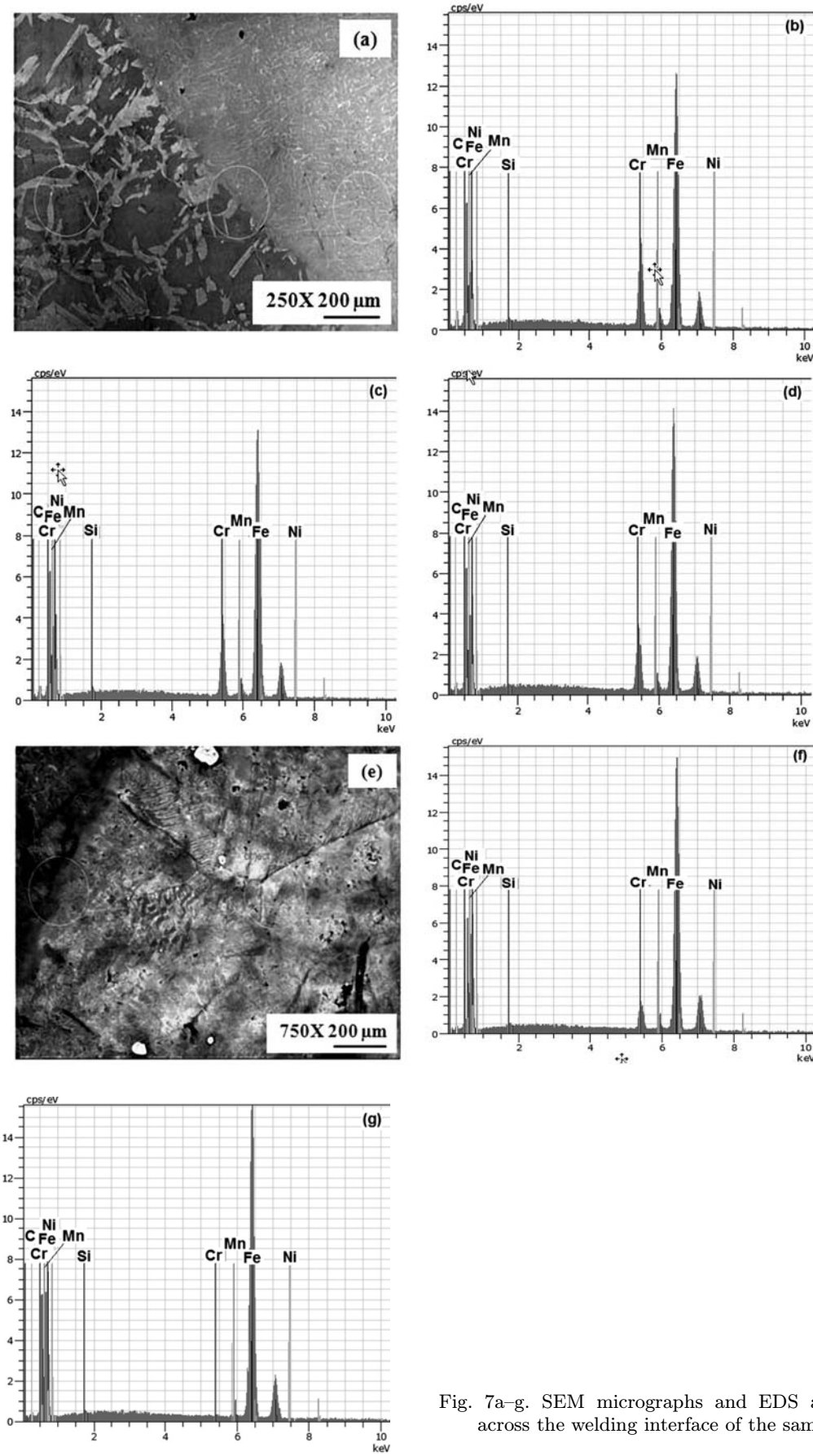

Fig. 7a–g. SEM micrographs and EDS analysis points across the welding interface of the sample S6.

Table 3. EDS analysis results of S3 and S6 samples

Sample No	Analysis points	Elements (wt.%)					
		C	Si	Cr	Mn	Fe	Ni
S3	1. point	0.13	0.39	15.05	2.92	79.44	0.88
	2. point	0.28	0.49	12.88	2.91	79.88	0.98
	3. point	0.13	0.28	7.48	2.58	87.52	0.80
	4. point	0.16	0.31	4.54	2.52	90.12	0.82
	5. point	0.11	0.24	0.54	2.17	95.10	0.83
S6	1. point	0.21	0.60	14.63	2.59	79.10	0.98
	2. point	0.15	0.47	13.09	3.09	80.85	0.96
	3. point	0.12	0.37	8.64	2.99	86.02	0.78
	4. point	0.11	0.37	4.48	2.53	90.59	0.87
	5. point	0.10	0.21	0.52	2.65	94.54	1.04

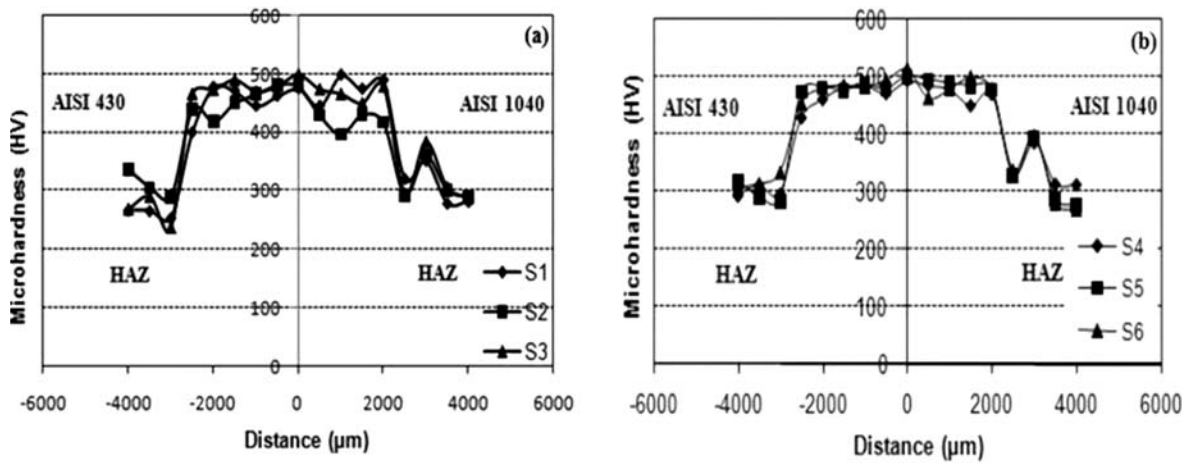

Fig. 8. Microhardness distribution across the welding interface of welded samples: a) S1–S3, b) S4–S6.

S3 and S6 are given in Table 3. The results of the elemental analysis and microstructural examination in the interface region of welded joints (samples S3, S6) clearly demonstrated that different amounts of Fe, Cr, C, Ni, Mn and Si were obtained. Additionally, from the results of EDS analysis taken from weld metal, HAZ-A and HAZ-B for the welded joints, it was revealed that the partially fused zone had high carbon content and also chrome carbides were precipitated in the form of grain boundary carbides. It was observed that the elemental chrome diffusion occurred towards AISI 1040 carbon steel from AISI 430 ferritic stainless steel, while elemental carbon diffusion took place within the same distance towards AISI 430 steel from AISI 1040 steel as seen in Figs. 6 and 7.

Microhardness measurements in the direction perpendicular to the weld interface of samples S1–S6 are given in Figs. 8a,b, respectively. As seen in these figures, significantly similar trend was observed in the microhardness profiles of all samples. The increase of hardness in the weld interface might be directly related to the microstructure formed in the weld interface. Formation of chrome carbide phases and a martensitic structure in the intermediate zone as a result of rapid cooling increased the hardness across the weld seam zone. Due to this result, higher microhardness values were observed across the weld seam. The highest hardness value achieved in the intermediate zone of weld metal was 515 HV for the sample S1. These higher hardness values for the weld metal were directly related to higher alloy content and low traverse speed, which resulted in both recrystallized carbides in the microstructure. For these samples, higher hardness values were reached on AISI 1040 side by increasing the welding current which can be claimed as the result of higher energy input. In addition, on AISI 1040 side, a drastic decrease was observed right at the edge of the seam, because this zone was carbon depleted and also partially fused. Consequently, in case of higher heat inputs and cooling rates, the hardness of the welding zone became higher, but the hardness values rose where no carbide formed and there was no effective diffusion of the welding zone due to the formation of martensite rises. From

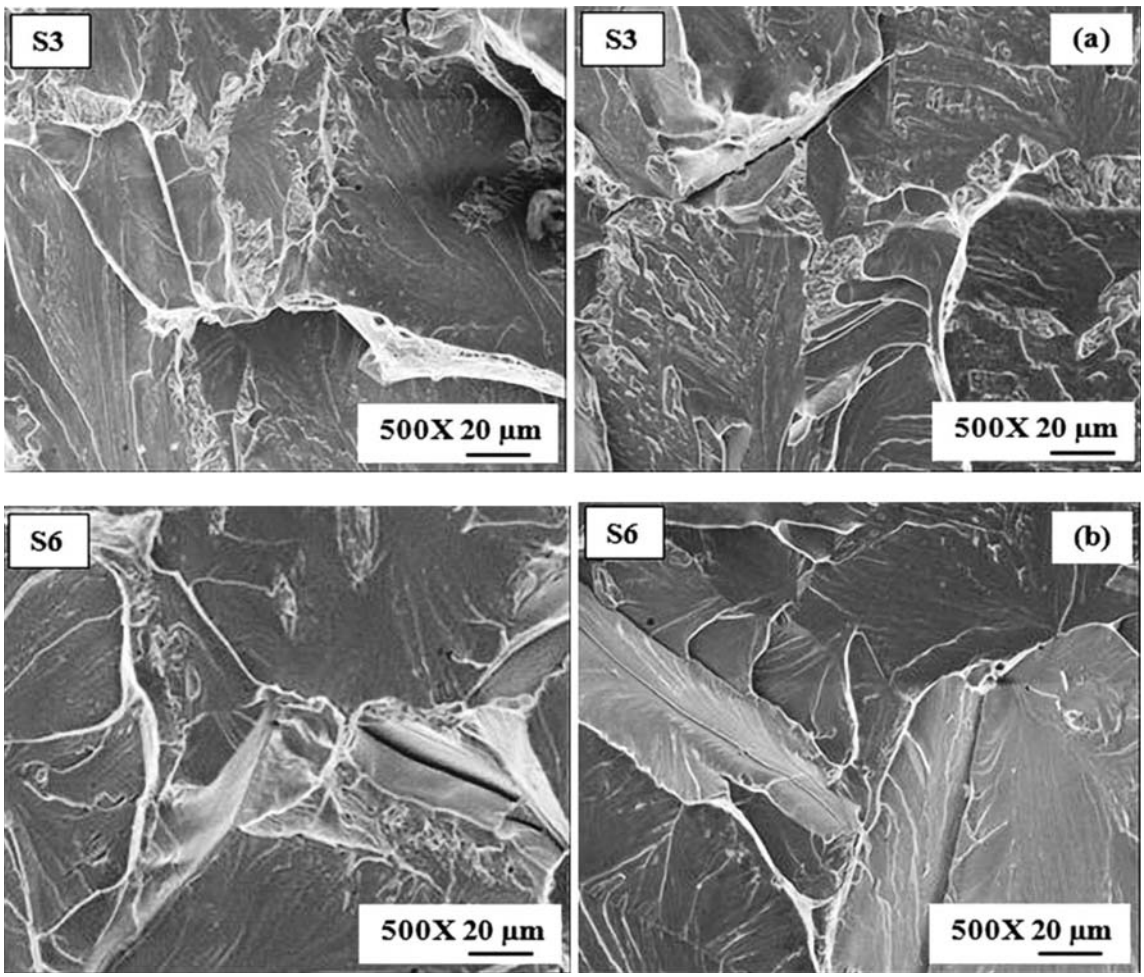

Fig. 9. SEM micrographs of fracture surfaces after notch impact test of welded samples: a) S3, b) S6.

the results of XRD analysis, CrC, $Cr_{23}C_6$, Cr_7C_3 and Cr_3C_2 compounds were observed on the welding metal of these welded joints.

With KPTA method ensuring higher energy input, a more uniform distribution of intensive carbide formation and presence of other hard phases in the microstructure positively affected the hardness. Furthermore, higher microhardness values obtained across the weld resulted from the incomplete dendritic structure formation in small proportions due to rapid cooling. It was considered that the decrease in hardness values across these zones resulted because of the diffusion of carbon on AISI 1040 side and the diffusion of chrome on AISI 430 side towards the welding metal, and owing to grain coarsening and concentration gradient, because said zones were under the influence of heat for an extended period of time depending on the energy input. This change was supported by the elementary concentration profile obtained from the EDS analysis on these zones. On AISI 430 side, it was observed that hardness increased slightly at a zone closely adjacent to the welding metal. From the microstructure images, it was understood that the increase in hardness was caused by the grain boundary carbides distribution and formation. Results obtained for all of the weld joints were similar to this structure.

3.2. Impact test

Examining the notch impact test results of the samples S1–S6, the maximum notch impact values were achieved in the samples welded at the small nozzle orifice diameter (S1 = 11.75, S2 = 13.75 and S3 = 14.25 J), while a decrease was observed in the notch impact values of samples (S4 = 5, S5 = 6 and S6 = 8 J) welded by increasing the nozzle orifice diameter gradually. Concurrently, depending on increasing nozzle orifice diameter, a decrease was noticed in the notch impact values of the welded joints. This may be attributed to the fact that the penetration depth increased due to higher temperatures and energy density resulting from increasing current intensity and a rise in heat. Also, this decrease in the notch impact toughness values was directly associated with the penetration depth, the presence of unwelded zones and structural changes that took place within the joining zone.

The existence and size of the unwelded section on the interface of the two metal pairs creates a notch effect, and therefore, they play a significant role in the behaviour of the notch impact tests carried out. Nozzle orifice diameter and welding current had a significant impact on the joining mechanism of the KPTA method, too. In addition, when a pair of two metals with high chrome and carbon contents is welded by means of the melting welding method, the precipitation of chrome carbide particles leads to hardening and causes brittleness. The fracture of the broken samples occurred on AISI 1040 side due to the formation of a martensitic structure.

3.3. Fractography

Figures 9a,b show the images of the fracture surfaces resulting from the notch impact test for the welded joints S3 and S6. Examining the fracture surface images, fractures resulting from the notch impact test were mostly on AISI 1040 side and it was observed that the broken grains had a crystalline fish backed appearance and the samples displayed a brittle fracture mechanism.

4. Conclusion

AISI 430/AISI 1040 dissimilar steels were joined by keyhole plasma arc welding technique using different nozzle orifice diameter. Following results were obtained:

1. The nozzle orifice diameter and energy input play a noteworthy role on the shape of keyhole and the penetration depth, weld metal width. The use of a higher energy input and small nozzle orifice diameter increased the penetration depth of KPTA welded joints.

2. The best penetration and keyhole are achieved with a nozzle diameter of 2.4 mm. The maximum penetration depth of 8 mm was obtained in sample 3. The increasing nozzle orifice diameter caused the decrease in the keyhole profile and the penetration depth.

3. The maximum strength values are achieved at a nozzle orifice diameter of 2.4 mm in the welded joints S1, S2 and S3. For these samples welded at a nozzle orifice diameter of 2.4 mm, the increase in the notch impact strength values is caused by the increase in the penetration depth due to high amounts of heat input occurring at small nozzle orifice diameter.

4. Depending on the increase in the nozzle orifice diameter, a reduction is observed in the notch impact strengths of the samples S4, S5 and S6 due to the existence of unwelded sections.

Acknowledgements

The authors wish to thank University of Fırat Research Fund for their support of this work under the FÜBAP-1500 project.

References

[1] Baeslack, B.: Welding brazing and soldering. Materials Park, OH, ASM Metals Handbook, *6*, 1993, p. 605.
[2] Craig, E.: Welding Journal, *67*, 1998, p. 19.
[3] Tomsic, M. J., Jackson, C. E.: Welding Journal, *53*, 1974, p. 109.
[4] Martikainen, J.: Journal of Materials Processing Technology, *52*, 1995, p. 68.
[5] Irving, B.: Welding Journal, *71*, 1992, p. 49.
[6] Lesnewich, A.: In: Weldability of Steels. 3rd ed. Eds.: Stout, R. D., Doty, W. D. New York, Welding Research Council 1978.
[7] Hsu, Y. F., Rubinsky, B.: International Journal Heat and Mass Transaction, *31*, 1988, p. 1409. doi:10.1016/0017-9310(88)90250-5
[8] Wang, Y., Chen, Q.: Jounal of Materials Processing Technology, *120*, 2002, p. 270. doi:10.1016/S0924-0136(01)01190-6
[9] Metcalfe, J. C., Quigley, M. B. C.: Welding Journal, *54*, 1975, p. 401.
[10] Halmoy, E., Fostervoll, H., Ramsland, A. R.: Weld World, *34*, 1994, p. 285.
[11] Teker, T., Ozdemir, N.: International Journal of Advanced Manufacturing Technology, 2012. doi:10.1007/s00170-011-3890-5
[12] Ureña, A., Otero, E., Utrilla, M. V., Múnez, C. J.: Journal of Materials Processing Technology, *182*, 2007, p. 624. doi:10.1016/j.jmatprotec.2006.08.030
[13] Teker, T.: Investigation of microstructure and mechanical properties of AISI 1040/AISI 430 steel couple welded by keyhole plasma welding technique. [Ph.D. Thesis]. Elazığ, Turkey, University of Fırat 2010.